Coherence-imaging spectroscopy for 2D distribution of ion temperature and flow velocity in a laboratory magnetosphere

K. Nakamura, M. Nishiura, N. Takahashi, Z. Yoshida, N. Kenmochi, T. Sugata, S. Katsura, and J. Howard

Citation: Review of Scientific Instruments **89**, 10D133 (2018); doi: 10.1063/1.5037124
View online: https://doi.org/10.1063/1.5037124
View Table of Contents: http://aip.scitation.org/toc/rsi/89/10
Published by the American Institute of Physics

REVIEW OF SCIENTIFIC INSTRUMENTS **89**, 10D133 (2018)

Coherence-imaging spectroscopy for 2D distribution of ion temperature and flow velocity in a laboratory magnetosphere

K. Nakamura,[1,a)] M. Nishiura,[1] N. Takahashi,[1] Z. Yoshida,[1] N. Kenmochi,[1] T. Sugata,[1] S. Katsura,[1] and J. Howard[2]

[1]*Graduate School of Frontier Sciences, The University of Tokyo, Kashiwa, Chiba 277-8561, Japan*
[2]*The Australian National University, Acton, ACT 2601, Australia*

(Presented 16 April 2018; received 20 April 2018; accepted 8 October 2018; published online 25 October 2018)

A coherence-imaging spectroscopy (CIS) technique was developed to investigate plasma confinement in a dipole system that imitates a planetary magnetosphere. Optical interference generated using birefringent crystals enables two-dimensional Doppler spectroscopy to measure ion temperatures and flow velocities in plasmas. CIS covers the entire dynamics of the pole areas as well as of the core and edge areas on a dipole confinement device. The two-dimensional visualization of these quantities in the magnetospheric-plasma device RT-1 was demonstrated using CIS. *Published by AIP Publishing.*
https://doi.org/10.1063/1.5037124

I. INTRODUCTION

Optical Doppler spectroscopy is generally used to diagnose the properties of ions, atoms, and molecules in discharge plasmas. Emissions from these particles are measured using a grating spectrometer that separates the light into spectral lines. The spectrometer obtains the one-dimensional (1D) spatial profile of temperatures and velocities from the Doppler effect. Based on the optical coherence effect,[1,2] coherence-imaging spectroscopy (CIS) enables us to obtain two-dimensional (2D) spatial images of temperatures and velocities in plasmas. Recently, the CIS has been successfully demonstrated on MAGPIE linear plasmas,[3] MAST spherical tokamak plasmas,[4,5] and DIII-D tokamak plasmas.[6–8] By applying CIS to the RT-1 laboratory-magnetosphere device, which simulates a planetary magnetosphere, we can elucidate the nature of self-organized plasmas and stable high-beta plasmas in a magnetosphere. In a dipole confinement device, we consider the visualization of a whole picture essential for understanding the confinement mechanism of self-organized plasmas. The toroidal flow is driven by drift forces, and plasma confinement is improved in the nonlinear regime of two fluid effects.[9] According to the experimental observation of a grating spectrometer in RT-1 plasmas, the toroidal flow is dominated by the $\boldsymbol{E} \times \boldsymbol{B}$ drift on the mid-plane. CIS covers the entire dynamics of the pole areas as well as of the core and edge areas on a dipole confinement device such as the RT-1, thereby helping us understand the whole dynamics of the dipole confinement system.

The RT-1 device imitates a planetary magnetosphere. It is intended to comprehend self-organized plasma confinement in a dipole topology both theoretically and experimentally.[9,10] The substantial physics is also applicable to advanced thermonuclear fusion experiments.[11] The RT-1 device confines the plasma in a dipole magnetic field produced by a levitated superconducting magnet. Electron-cyclotron heating (ECH) produces and sustains a stable high-beta plasma (in which the ratio of electron pressure to magnetic pressure exceeds unity).[12] Based on the diamagnetic signal and the plasma equilibrium obtained by solving the Grad–Shafranov equation, the high-beta plasma is largely populated by high-energy electrons with energies of a few tens of keV.

Ion dynamics in the RT-1 device are measured using multi-chord spectroscopy, and the ion temperatures of the horizontal and vertical chords have anisotropic features.[13] Ion-heating experiments have been performed using a slow wave excited by using a double-loop antenna from a high-field area near the pole. The excited wave propagates toward low-field areas and is absorbed at the ion-cyclotron layers. This scenario of direct ion heating has been demonstrated successfully by a measured increase in the ion temperature.[12] To visualize the ion dynamics, i.e., the ion temperatures and flow velocities in magnetospheric plasma, we recently implemented CIS on the RT-1 device.

II. COHERENCE-IMAGING SYSTEM FOR RT-1 PLASMAS

The CIS system comprises a camera (Canon EOS 70D), a CIS cell, and three lenses (Fig. 1). The camera is equipped with a complementary metal oxide semiconductor (CMOS) image sensor (5472 × 3648 pixels). The input signal to the camera is generated by a field programmable gate array synchronized with the main trigger for the RT-1 control system. The input signal controls the camera shutter. The objective lens (lens 1:

Note: Paper published as part of the Proceedings of the 22nd Topical Conference on High-Temperature Plasma Diagnostics, San Diego, California, April 2018.
a)Electronic mail: nakamura.kaori17@ae.k.u-tokyo.ac.jp.

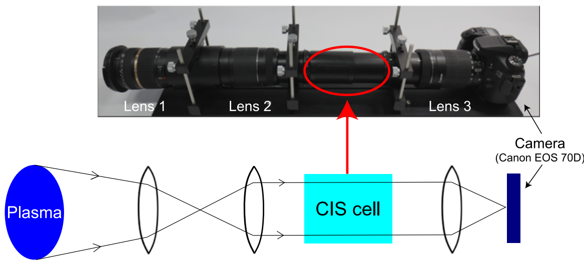

FIG. 1. CIS system setup for the RT-1 device.

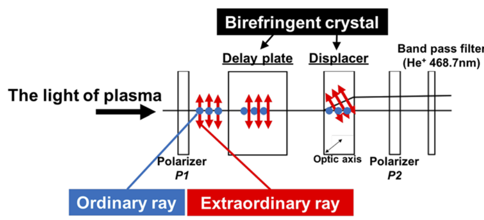

FIG. 2. The CIS system (inside the CIS cell drawn in Fig. 1). The dots and arrows indicate the ordinary and extraordinary waves, respectively.

10–24 mm; F/3.5–4.5) views a wide angle (108°–60°). The pair of lenses 2 and 3 (18–300 mm; F/3.5–6.3) transmit the light from lens 1 to the CMOS image sensor. The CIS cell is inserted between lens 2 and lens 3 to produce the optical interference. The fringe pattern appears on the plane of the CMOS image sensor.

The CIS cell (Fig. 2) comprises an interference filter with a passband at 468.6 nm and a half-bandwidth of 1.8 nm, a pair of polarizers, a delay plate, and a displacer. The delay plate and the displacer are made of α-BBO crystals (α−barium borate, BaB_2O_4) with an α cut and a 45° cut, respectively. Polarizer $P1$ filters unpolarized light and passes linearly polarized light. When the linearly polarized light enters the delay plate, the orientation of the light polarized at 45° to the optical axis of the delay plate produces a phase difference between the ordinary and extraordinary rays. The displacer transversely separates the light into two rays, which are focused on the CMOS image sensor by using lens 3. The thicknesses of the delay plate and the displacer are chosen as 15 and 3 mm, respectively. The design is determined for target plasmas in the ranges of T_{i} from a few to 100 eV and of V_{i} that are less than a few 10 km/s.

A typical emission spectrum from RT-1 plasma is plotted in Fig. 3. The light from He II (468.6 nm) in the spectrum passes through the interference filter, which rejects unwanted light from C III (~465 nm) and He I (471.3 nm). Seen the background at this spectrum, it is found that the background level due to the Bremsstrahlung emission is negligibly small (less than 1/1000) compared with the He^+ emission. These line ratios change with the discharge conditions.

The CMOS image sensor captures the interferogram, which is analyzed to determine the ion temperature and the flow velocity. The interference fringe is given by[2]

$$S = I_0\left[1 + \zeta_I \zeta \cos(\phi_I + \phi)\right], \tag{1}$$

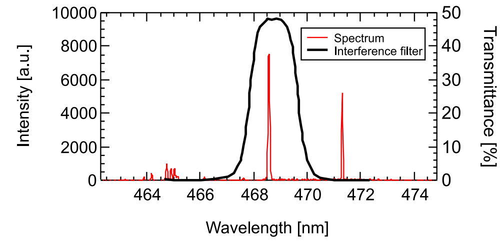

FIG. 3. Typical spectrum of helium plasma and transmittance of the interference filter (bandpass filter).

where I_0 is the brightness, ζ is the contrast, and ϕ is the phase shift. The quantities ζ_I and ϕ_I are the instrumental fringe contrast and phase, respectively. For light of wavelength λ, $\phi_0 = 2\pi L B(\lambda)/\lambda_0$ is the offset in the phase delay produced by a delay plate of thickness L and birefringence $B(\lambda) = n_E(\lambda) - n_O(\lambda)$. The birefringence can be expressed by the refractive indices for the ordinary ray $n_o(\lambda)$ and the extraordinary ray $n_E(\lambda)$, and it is comparable to the optical coherence length of the Doppler-broadened line. The instrumental phase is defined as $\phi_I \equiv \phi_S + \phi_0 + k_0 x$, where the wavenumber is given by $k_0 = 2\pi d/f_{lens}\lambda_0$, in terms of the focal length f_{lens} of the camera lens and the ray displacement d in the displacer plate. The first term can be corrected using a Zn lamp and integrating sphere. The calibration procedure is described in Sec. III D. The second and third terms are derived from the linear phase approximation. We set $\zeta_I = 1$ and $\phi_S = 0$ as the normalization.[2]

To separate I_0 from the interferogram, we demodulated the measured fringe pattern image using the Hilbert transform based on the fast Fourier transform (FFT). The Doppler parameters are associated with the contrast and the phase[2]

$$\zeta = \exp\left(-\frac{T_i}{T_c}\right), \tag{2}$$

$$\phi = \phi_0\left(1 + \kappa \boldsymbol{V_i} \cdot \hat{\boldsymbol{l}}\right). \tag{3}$$

The characteristic temperature T_c is given by $k_B T_c = 2 m_i c^2/\widehat{\phi_0}^2$, where m_i is the mass of the ion, k_B is Boltzmann's constant, c is the speed of light, and $\widehat{\phi_0} = \kappa\phi_0$ is the group phase delay, with the constant κ accounting for the chromatic dispersion of the birefringent crystal. In the present RT-1 experimental conditions, the magnetic field where we diagnosed is less than 0.1 T. The Zeeman effect is negligible. The Doppler effect is the main mechanism to broaden the line spectrum of He^+. The measured quantities are line integrated T_{i} and V_{i}, although we must treat the effect on the inner product of the ion flow velocity $\boldsymbol{V_i}$ and sightline vector $\hat{\boldsymbol{l}}$ for the local quantities.

III. EXPERIMENTAL SETUP

A. RT-1 device

Figure 4 shows the cross sections of the RT-1 device.[9,12–14] The vacuum vessel is 1 m in radius. The

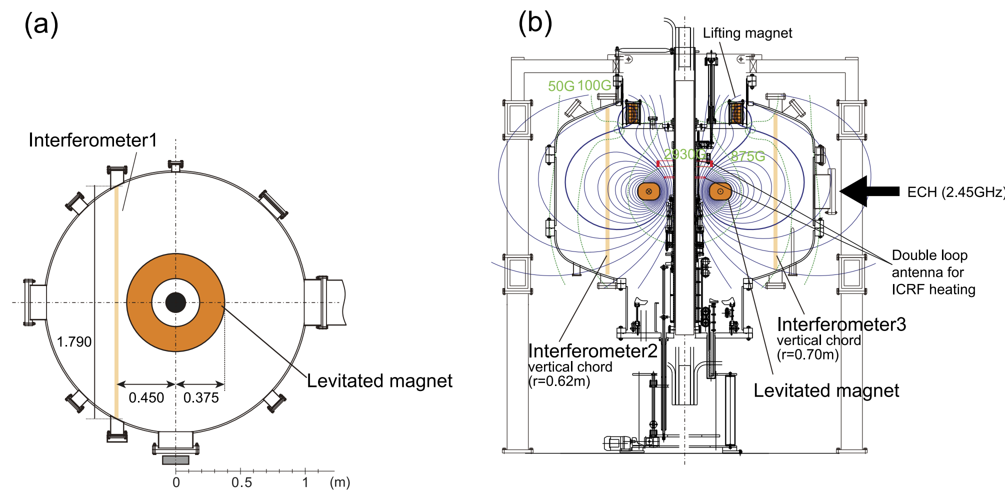

FIG. 4. Cross-sectional view of (a) a mid-plane and (b) the vertical section of the RT-1 device.

levitated superconducting ring magnet (dipole field magnet) has an outer radius of 0.375 m, is cooled down to <20 K in the vacuum vessel, and is levitated by a normally conducting magnet outside the vacuum vessel. For the cross section in Fig. 4, we define the cylindrical coordinates (r, z) with toroidal symmetry. The levitated magnet is positioned by feedback control at the mid-plane ($z = 0$) during plasma experiments and produces the dipole magnetic field for plasma confinement.[9] Helium plasmas are produced and heated by ECH using 2.45-GHz microwaves. The nominal ECH output power is 20 kW, and the discharge duration is 1 s.

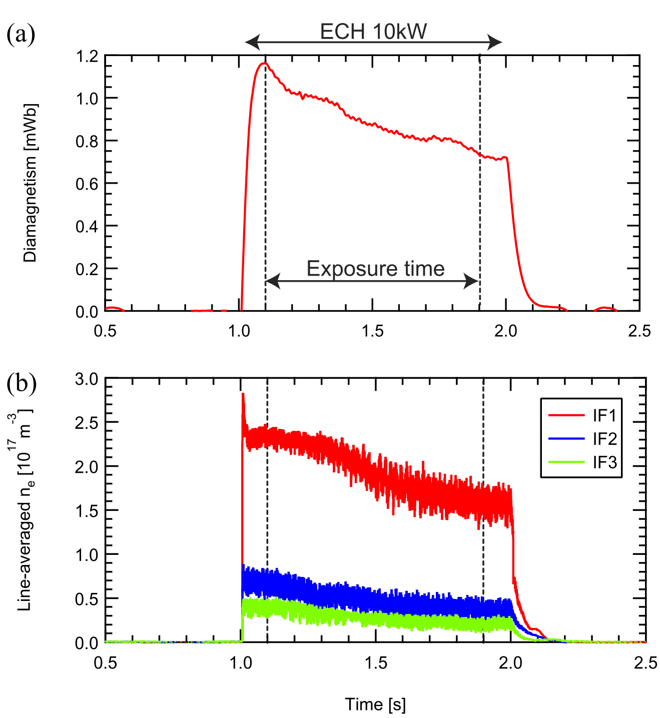

FIG. 5. Discharge waveforms of (a) the diamagnetic signal and (b) the line-averaged density at $r = 0.45$ m (IF1), $r = 0.62$ m (IF2), and $r = 0.72$ m (IF3).

B. Main diagnostics of RT-1

We use 75-GHz interferometers to measure the line-averaged electron densities at three chords (see Fig. 4): IF1 at $r = 0.45$ m (horizontal direction), IF2 at $r = 0.62$ m (vertical direction), and IF3 at $r = 0.72$ m (vertical direction). By reconstructing these quantities, the electron density at the peak lies in the range 10^{17}–10^{18} m^{-3} in Ref. 12. The diamagnetic signal from the plasma is measured by magnetic loops. The beta value is determined from the diamagnetic signal and the plasma equilibrium by solving the Grad–Shafranov equation.

Figure 5 shows the line-averaged densities and the diamagnetic signal in RT-1 plasma. The ECH power at 2.45 GHz is 10 kW, and the filling gas pressure of helium is 0.6 mPa. The local electron beta is ∼20% for this case.

C. Coherence-imaging spectroscopic system and grating spectrometer at RT-1

Figure 6 shows a cross-sectional view at the mid-plane of the RT-1 vacuum vessel with the fields of view: CIS and the grating spectrometer range are indicated in light blue and in

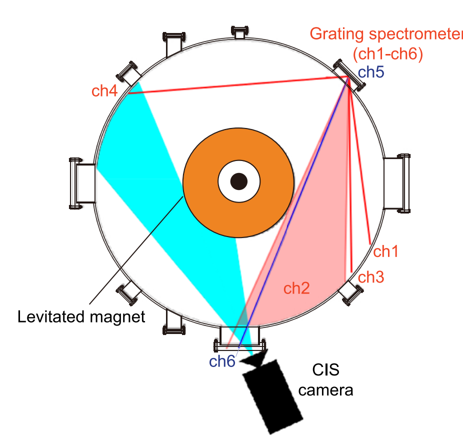

FIG. 6. Fields of view of the CIS system and the grating spectrometer at the mid-plane of RT-1.

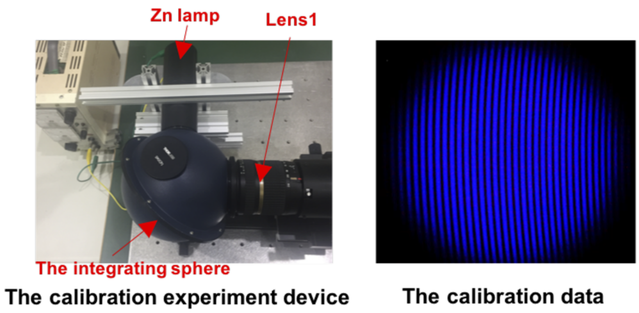

FIG. 7. A Zn lamp is used for the CIS calibration experiment (left). The interferogram (right) is obtained with an exposure time of 30 s.

red, respectively. A Czerny–Turner spectrometer (1 m focal length, 2400 grooves/mm grating, and 0.55 nm/mm reciprocal linear dispersion) equipped with a charge-coupled device detector (1024 × 256 pixels) is used. The CIS data are usually compared with the radial profile of the ion temperature, and the flow velocity is measured using the grating spectrometer in the equatorial plane. The channel, ch2, scans the range of tangent radii $375 < r < 925$ mm horizontally. We use ch5 and ch6 to measure the same radial position but facing each other (see Fig. 6). These two channels are used to determine the zero point of the flow velocity.

D. Calibration of the CIS system

To obtain the instrumental fringe contrast ζ_I and the phase ϕ_I, the CIS is calibrated using a light source. We introduced a Zn lamp (468.014 nm)[15] into an integrating sphere to provide uniform illumination to the object lens (lens 1) of the CIS system. The wavelength of the lamp is close to the He II emission at 468.6 nm. The setup for the calibration experiment and the measured interferogram are shown in Fig. 7. The image data are acquired with an exposure time of 30 s. Only the blue pixels are analyzed using FFT in the raw image containing red-green-blue (RGB) data. The contrast and the phase determine the limit of instrumental resolution and the zero levels. The calibration procedure is performed both before and after the plasma experiments.

IV. ION TEMPERATURE AND FLOW VELOCITY FROM CIS

We used CIS to measure the line-integrated profiles of intensity, ion temperature, and flow velocity for an RT-1 plasma discharge. The camera shutter was open from $t = 1.1$ to 1.9 s, whereas the grating spectrometer was active from $t = 1.2$ to 2.0 s. Figure 8 shows the line-integrated one-dimensional profiles of I_0, T_i, and V_i at the mid-plane (z = 0), as measured via CIS; the line-integrated two-dimensional profiles are shown later. The data from the grating spectrometer were accumulated from four shots, whereas CIS required only one shot. The relatively low input power of ECH produced a low density of He^+.

The ion flow velocities from CIS and from the grating spectrometer are both of the order of ∼7 km/s, which agree with each other within the error bar. The CIS and the grating spectrometer measure the same line of sight. But the optics between the CIS and the grating spectrometer are different. Therefore, more work has to be performed before we can claim that the diagnostic has been validated. The slow ion flow velocities under these conditions are caused by the low input power of the ECH. In the past experiments, the ion flow velocities at the mid-plane were found to increase up to approximately a few tens of km/s, depending on the ECH power.

The two-dimensional profiles from CIS are shown in Fig. 9. The lower part of the double-loop antenna for ion-cyclotron-resonance heating[13] is located at the upper side of the levitated magnet. The intensity of He II 468.6 nm increases along the magnetic-field lines near the levitated magnet.

From the profile of T_i, we find that T_i is uniformly distributed in the confinement region, except for a cold region near the levitated magnet at r = 0.4–0.5 m on the mid-plane. For the intensity and temperature, the vertical fringes remain in the analyzed images owing to the demodulation of the DC component. We consider that a sudden change in plasma parameters in a fringe contains a large error, which makes the separation of the DC component difficult. Increasing the number of fringes at the same view solved this

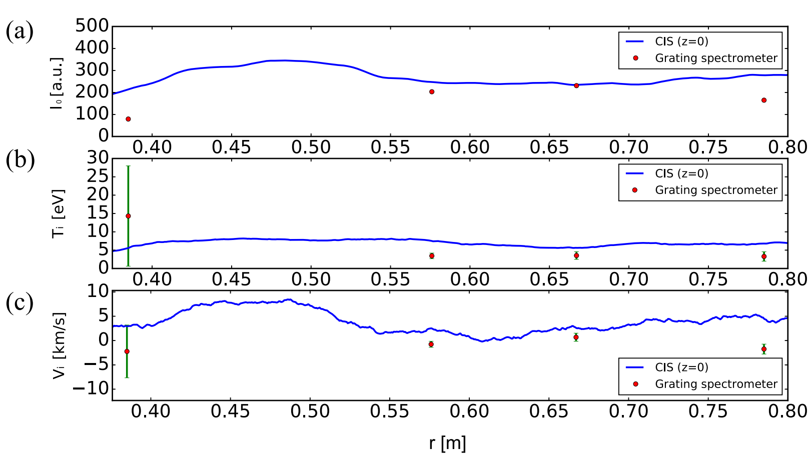

FIG. 8. The profiles of (a) intensity, (b) ion temperature, and (c) flow velocity of the RT-1 plasma. The data measured by the grating spectrometer are shown as filled circles.

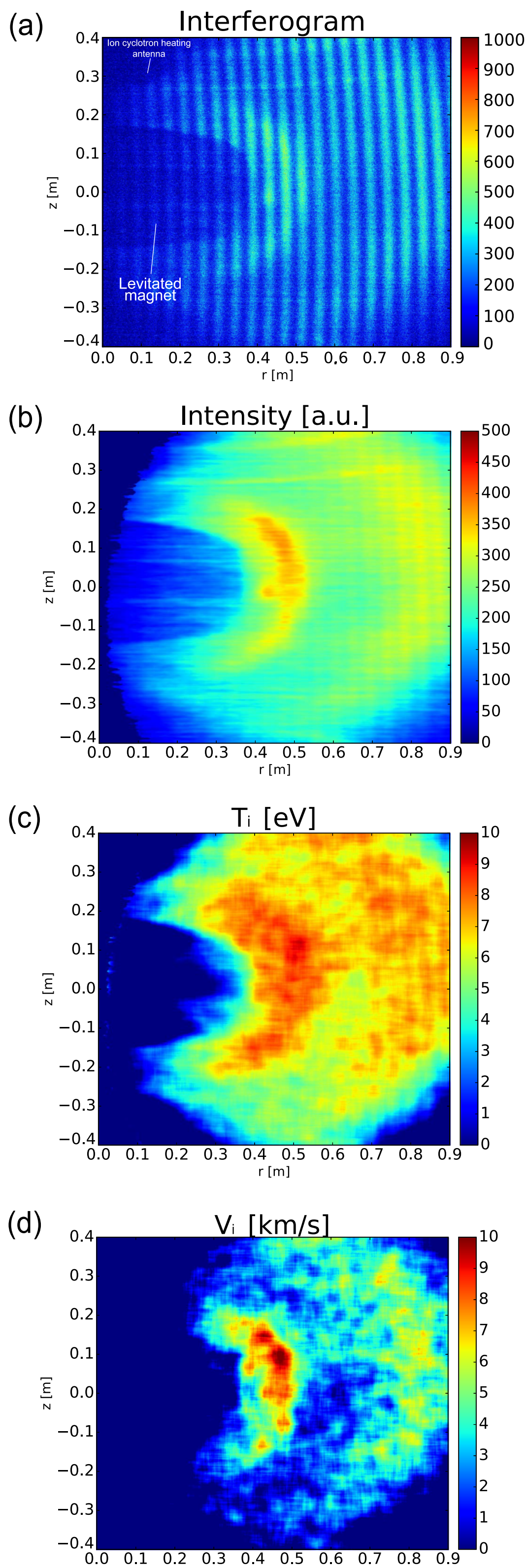

FIG. 9. Line-integrated 2D profiles of (a) interferogram, (b) brightness, (c) ion temperature, and (d) ion flow velocity measured in the RT-1 helium plasma. The measured images are converted to the mirror-reversed images. The positive flow is defined as the clockwise (ion diamagnetic) direction when a plasma is viewed from the upper side of the RT-1.

problem by lengthening the focus of the lens 1 optics, i.e., changing the field of view. As different discharge conditions may change the RT-1 profiles completely, further studies are essential to understand the confinement of magnetospheric plasmas.

The CIS images were analyzed using two calibration data with the interval of 120 min. The influence on the instrumental conditions was investigated within this time scale. In the case of the analyzed results for Fig. 9, the ion temperature and the flow velocity changed at most within 0.4 eV and 500 m/s, respectively.

V. SUMMARY

We developed CIS to measure ion dynamics in magnetospheric plasmas produced in RT-1. This experiment successfully demonstrated for the first time the visualization of 2D ion temperatures and flow velocities in magnetospheric plasma.

ACKNOWLEDGMENTS

This work was supported by JSPS KAKENHI Grant No. 17H01177 and the NIFS Collaboration research program (No. NIFS15KOAH034).

[1] J. Howard, C. Michael, F. Glass, and A. Danielson, Plasma Phys. Controlled Fusion **45**, 1143–1166 (2003).
[2] J. Howard, C. Michael, H. Chen, R. Lester, A. Thorman, and J. Chung, J. Instrum. **10**, P09023 (2015).
[3] R. Lester, Y. Zhai, C. Corr, and J. Howard, Plasma Sources Sci. Technol. **25**, 015025 (2016).
[4] I. Waters, H. Frerichs, S. Silburn, Y. Feng, J. Harrison, A. Kirk, and O. Schmitz, Nucl. Fusion **58**, 066002 (2018).
[5] S. A. Silburn, J. R. Harrison, J. Howard, K. J. Gibson, H. Meyer, C. A. Michael, and R. M. Sharples, Rev. Sci. Instrum. **85**, 11D703 (2014).
[6] J. Howard, A. Diallo, M. Creese, B. Blackwell, S. L. Allen, R. M. Ellis, G. D. Porter, W. Meyer, M. E. Fenstermacher, N. H. Brooks, M. Van Zeeland, and R. L. Boivin, Rev. Sci. Instrum. **81**, 10E528 (2010).
[7] T. R. Weber, S. L. Allen, and J. Howard, Rev. Sci. Instrum. **83**, 10E102 (2012).
[8] C. M. Samuell, G. D. Porter, W. H. Meyer, T. D. Rognlien, S. L. Allen, A. Briesemeister, A. G. Mclean, L. Zeng, A. E. Jaervinen, and J. Howard, Phys. Plasmas **25**, 056110 (2018).
[9] Z. Yoshida, S. M. Mahajan, T. Mizushima, Y. Yano, H. Saitoh, and J. Morikawa, Phys. Plasmas **17**, 112507 (2010).
[10] Z. Yoshida, Y. Ogawa, J. Morikawa, S. Watanabe, Y. Yano, S. Mizumaki, T. Tosaka, Y. Ohtani, A. Hayakawa, and M. Shibui, Plasma Fusion Res. **1**, 008 (2006).
[11] A. Hasegawa, L. Chen, and M. E. Mauel, Nucl. Fusion **30**, 2405 (1990).
[12] M. Nishiura, Z. Yoshida, H. Saitoh, Y. Yano, Y. Kawazura, T. Nogami, M. Yamasaki, T. Mushiake, and A. Kashyap, Nucl. Fusion **55**, 053019 (2015).
[13] M. Nishiura, Y. Kawazura, Z. Yoshida, N. Kenmochi, Y. Yano, H. Saitoh, M. Yamasaki, T. Mushiake, A. Kashyap, N. Takahashi, M. Nakatsuka, and A. Fukuyama, Nucl. Fusion **57**, 086038 (2017).
[14] Y. Kawazura, Z. Yoshida, M. Nishiura, H. Saitoh, Y. Yano, T. Nogami, N. Sato, M. Yamasaki, A. Kashyap, and T. Mushiake, Phys. Plasmas **22**, 112503 (2015).
[15] See https://physics.nist.gov/PhysRefData/ASD for NIST atomic spectra database lines.